ESCUELA DE CONSTRUCCIÓN CIVIL
FACULTAD DE INGENIERÍA
Revista de la Construcción
Journal of Construction

Research Article

Effect of silica fume and basalt fibers on the fracture parameters of magnesium phosphate cement incorporating fly ash

Ahmet Onur Pehlivan[1,*]

[1] Assistant Professor, Department of Civil Engineering, Maltepe University, 34857, Maltepe, Istanbul, (Türkiye), onurpehlivan@maltepe.edu.tr
*Correspondence: onurpehlivan@maltepe.edu.tr

Received: 02.07.2021; **Accepted:** 19.12.2022; **Published:** 29.12.2022

Citation: Pehlivan, A. (2022). Effect of Silica Fume and Basalt Fibers on the Fracture Properties of Magnesium Phosphate Cement Incorporating Fly Ash. Revista de la Construcción. Journal of Construction, 21(3), 523-538. https://doi.org/10.7764/RDLC.21.3.523.

Abstract: Magnesium phosphate cements are implemented for several purposes demonstrating significant mechanical properties in limited durations. However, brittle behavior of this material needs utmost concern and tensile performance may be enhanced with the proper application of fibers increasing both ductility and energy absorption capacity. This research studies the effect of basalt fibers (BF) and silica fume (SF) on the fracture parameters of magnesium phosphate cement (MPC). MPC mortar mixtures were prepared with different SF (0, 5, 10%) and BF amounts (0, 0.5, 0.75, 1 % by wt.). Also fly ash was adopted with a constant ratio for all mixes. Compressive strength and splitting tensile strength results indicated that addition of SF into mixtures extensively developed the matrix structure and improvements were noted with the increasing SF content. The inclusion of BF enhanced the flexural behavior although there were significant improvements in the fracture energy as well as the double-K parameters. Improvements in the tensile capacity of specimens with high BF were prone to the amount of SF percentage such that inclusion of 1 % BF performed best with 10 % SF added mixtures. Load-CMOD (crack mouth opening displacement) curves obtained from notched three-point tests were given for all specimen series and parameters were calculated according to the double-K criterion. Addition of BF resulted in higher toughness values however presence of SF was very significant in establishing appreciable development in toughness values. Brittleness index was implemented to establish clear conclusions on the findings and best performance was seen for specimens with 10% SF and 1% BF.

Keywords: Magnesium phosphate cement, basalt fiber, notched fracture test, silica fume, double-K criterion

1. Introduction

Magnesium phosphate cement (MPC) is a relatively new kind of acid-base cementitious material formed by mixing dead burned magnesia with a phosphate source within the presence of a retarding additive for proper compaction. MPC has special binding abilities that can be facilitated as a fast repair material in various fields of application like stabilization of toxic wastes, wastewater treatment and dental operations (Zhang et al., 2017; Han et al., 2020).

In comparison with the traditional portland cement, MPC exhibits superior characteristics in extremely rapid setting, very high early strength, being able to set at very low temperatures, excellent durability, good adhesion for creating quality com-

posites, near natural pH and low drying shrinkage. Such good cementing abilities possess significant advantages in the construction sector for rapid repairs of facilities of extreme importance such as bridges, airport runways and highways. (Li & Chen, 2013; Mo et al., 2018).

MgO is the primary ingredient of MPC and its calcination temperature has a significant impact on the hydration products as well as the hydration behavior such as setting time. The calcination temperature of MgO affects the setting time altering the borate absorption efficiency by changing the immobilization mechanism (Sasaki & Moriyama, 2014).

Retarders should be added to supply enough time to increase the time of mixing and homogenous internal structure. Hall et al. (2001) compared borax, sodium tripolyphosphate and boric acid and highlighted borax as the most efficient retarder. A higher amount of borax was found to be increasing the setting time (Yang et al., 2014). Borax was found helpful in delaying the reactions by the formation of a polymeric coating on the surface of MgO grains thus hampering the MgO dissolution and increasing the bonding time (Riberio et al., 2019). Therefore, the amount of retarder should be adjusted concerning MgO amount rather than the overall MPC mixture weight.

Although MPC mixtures have outstanding mechanical characteristics, they exhibit high brittleness with a shallow strain capacity. This poor behavior may be improved by reinforcing the mixtures with a wide range of fibers employed according to chemical coherence and low pH values of MPC mixtures. In latest years, BF gained significant attention as a decent reinforcement tool which originates naturally and besides its low cost, has several mechanical advantages like excellent high temperature performance, high tensile strength and high modulus of elasticity. (Ahmad & Chen, 2020; Aminul Haque et al., 2020; Qin et al., 2018; Fang et al., 2018; Sateshkumar et al., 2018). Also in another study, basalt fibers were used along with steel fibers as hybrid fibers and such usage was found to be successive considering the increase in energy absorption and flexural toughness (Jenifer and Berindha, 2021). Recycled propylene fibers were also found to be increasing the flexural toughness and longer fibers were found to be more effective (Araya-Letelier et al., 2019).

MPC mixtures were reported to have disintegration problems when they come in contact with water. Fly ash was found helpful when increasing water resistance and also increasing the mechanical strength (Mo et al. 2018). SF is another cement replacement material widely used in cementitious mixtures creating a good bond with the aggregate interface and excellent microfilling effect. However, there is a lack of studies on the impact of SF on MPC mixtures and the possible improved bonding of the BF with the inclusion of SF (Ahmad & Chen, 2020). The effect of SF and BF should have been investigated on the ductility and toughness behavior of MPC mixtures. To employ the toughness measurements, flexural loading was conducted on the notched beam specimens to determine the needed results to conduct the double-K criterion (Xu & Reinhardt, 2000; Xu & Reinhardt 1999) which was found to be promising when dealing with energy dissipation characteristics of different samples minimizing the effect of the specimen size. Hence, detailed mechanical performance of MPC mixtures enhanced with SF addition and reinforced with varying amounts of BF was investigated in this study.

2. Materials and methods

2.1. *Materials*

Fiber-reinforced MPC mortars were prepared by combining dead burned magnesia and mono ammonium dihydrogen phosphate (ADP) with different molar ratios. Also fly ash and SF were used as extra binders since they have been useful for the overall integrity of MPC matrix and also decreased the total cost of the binder. River sand with a maximum size of 2 mm and tap water were used for mortar specimen preparation. BF with 9-23 µm diameter were used with 12 mm fiber length. Properties of BF are given in Table 1 and properties and compositions of binder materials are shown in Table 2. Magnesia was composed of more than 90% of MgO and SF had 96% SiO_2. Borax was used as a set retarder to elongate the mixing time necessary for proper handling and casting by delaying the hydration mechanism.

Table 1. Properties of BF.

Material	BF
Diameter (μm)	9-23
Length (mm)	12
Tensile Strength (MPa)	4840
MOE (GPa)	89
Density (kg/m^3)	2700

Table 2. Properties and compositions of MPC ingredients.

Composition	Magnesia (%)	Fly Ash (%)	SF (%)	ADP (%)	Borax (%)
MgO	90.9	2.06	0.43	> 99	> 98
SiO_2	3.9	52.56	96.31		
Al_2O_3	2.3	26.46	0.91		
Fe_2O_3	1.2	6.77	0.42		
CaO	1.3	2.24	0.78		
SO_3	-	0.2	-		
Na_2O	-	0.38	-		
K_2O	-	4.22	-		
LOI	-	3.3	1.2		

Table 3. Mixture proportions

Mixtures	MgO	ADP	Fly Ash	SF	BF	Borax	Sand	Water
Control	1000	475	369	0	0	100	972	350
BF0.5	1000	475	369	0	16.48	100	980	353
BF0.75	1000	475	369	0	24.81	100	984	354
BF1.00	1000	475	369	0	33.23	100	989	356
S5	1000	475	369	92	0	100	1018	367
S5BF0.50	1000	475	369	92	17.25	100	1027	370
S5BF0.75	1000	475	369	92	25.98	100	1031	371
S5BF1.00	1000	475	369	92	34.78	100	1035	373
S10	1000	475	369	184	0	100	1064	383
S10BF0.50	1000	475	369	184	18.56	100	1162	418
S10BF0.75	1000	475	369	184	28.39	100	1218	438
S10BF1.00	1000	475	369	184	38.71	100	1279	460

2.2. *Mixing*

MPC mixtures were formed by mixing MgO powders, $NH_4H_2PO_4$ (ADP), fly ash, SF and BF in Hobart mortar mixing device. Three different SF ratios (0, 5, 10 by weight of total binder) and three different BF ratios (0, 0.5, 0.75, 1% by wt.) were used. Borax percentage was selected as 10% of the weight MgO powders and fly ash was used as the 20% of the total MPC binder weight. Mortar specimens were prepared with 1:0.18:0.50 by weight of MPC, water and sand, respectively. Mixture proportions are given in Table 3. All ingredients except water were mixed in dry condition for 120 seconds with Hobart mixture including sand, fly ash, MgO, ADP and borax. Then water was added gradually in 30 seconds and mixing process was continued for 90 seconds more. Finally, fibers were added slowly to provide optimum dispersion in 60 seconds and further mixing was performed for 60 seconds more. Mixtures without fibers were mixed for a total of 4 minutes. Totally, a mixing procedure of 6 minutes was conducted.

A total of 12 mix types were formed and a total of 24 prismatic specimens with 50 x 100 x 500 mm for notched flexural tests, 72 cubic specimens with 40 x 40 x 40 mm for compressive strength tests (6 replicates for each mix type) and 36 cubic specimens with 50 x 50 x 50 mm (3 replicates) for splitting tensile strength were cast. All specimens were stored in a humidity room with 22 ±1 ºC and 50 ±5 % RH.

Flowability of fresh reinforced pastes was obtained in accordance with the ASTM C1437 (2015) standard. On the jumping table, mortar mixtures were placed as two layers in a steel flow mold with a full height of 50 mm and were tapped 20 times for both layers. When flow mold was lifted, flow table test was conducted by applying 25 strokes to the molded mixture in 15 seconds. Flow values were calculated by the average of the two measurements along the perpendicular directions to determine the flowability of cement mortars.

Mechanical tests consist of compressive strength tests on and splitting tensile strength tests were performed on cubic specimens and notched flexural strength tests were conducted on prismatic specimens. Compressive strength tests were performed on cubic specimens and splitting tensile tests on cylindrical specimens due to specifications given in ASTM C39 (2021) and ASTM C496 (2017), respectively. Cubic specimens were crushed under a loading rate of 500 N/s whereas splitting tensile tests were conducted at a loading rate of 100 N/s and splitting tensile strength was calculated with the expression in Eq. 1.

$$f = \frac{2P}{\pi a} \tag{1}$$

where P and a are the maximum load and dimension of cube specimens, respectively.

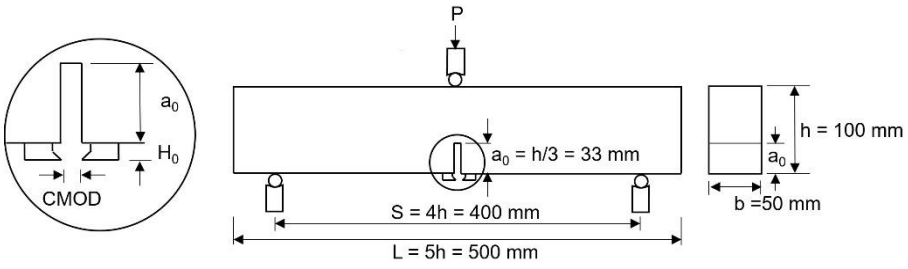

Figure 1. Scheme of the notched three-point loading.

Flexural toughness results of notched prismatic specimens were calculated according to given specifications in RILEM FMC-50R (1985). The scheme of the three-point notched flexural loading is shown in Figure 1. Span length to height of the specimen were 4 and depth of the notch was selected to 1/3 of the overall height as 33 mm. Three-point bending was applied on the specimens with a clear span length of 400 mm by a controlled closed loop servo hydraulic test system with a maximum loading capacity of 100 kN at a rate of 0.01 mm/min. Clip on displacement gauge was attached on prismatic specimens with

the steel knife edges glued to the sides of the notch at the midcenter. Also, two linear variable transducers were mounted at each side of the prismatic specimens to record the vertical deflection and record simultaneously with all the other data. To eliminate any risk of crushing the attached equipment, the test was terminated when a crack mouth opening displacement value of 0.2 mm was reached for all specimen types.

2.3. *Calculation of fracture energy*

Fracture energy is the amount of absorbed energy per unit area in the crack extension direction. Hillerborg (1976) proposed a standard method for calculating the fracture energy with a notch in the bottom midsection of a prismatic specimen. Fracture energy can be calculated as the ratio of the total area under the load-CMOD curve of the notched beam to the total crack ligament area as given in RILEM FMC-50R (1985) with Eq. 2.

$$G_f = \frac{W_0}{A} = \frac{W_0}{b(h - a_0)} \tag{2}$$

where W_0 stands for the area under the load-deflection curve which also represents the work done by the external force applied on the notched beam and A is the ligament area.

2.4. *Calculation of fracture energy*

Fracture behavior of concrete is significantly influenced by the fracture process zone. Many researchers have proposed several models to simulate the softening behavior and fracture characteristics in concrete applications. According to Xu & Reinhardt (2000), fracture process zone consists of three distinct stages: (i) crack initiation, (ii) stable crack propagation, (iii) unstable fracture, as was also manifested in several other studies. To solve the analytical solution of the fictitious crack for quasi brittle materials, a double K is proposed by Xu & Reinhardt. (1999). In double–K criterion, two fracture parameters were introduced for different stages of the fracture mechanism and both of them are given in terms of stress intensity factor. K^Q_{IC} is called the initiation toughness whereas K^S_{IC} is the unstable fracture toughness or the critical stress intensity factor. Initiation toughness, K^Q_{IC}, is calculated by determining the initial cracking load (P_Q) from the loading sequence and initial crack length, a test parameter decided prior to testing. Unstable fracture toughness, K^S_{IC}, is calculated by obtaining the maximum load P_{max} and deriving the critical effective crack length. Crack initiation and propagation phases may be followed by checking the toughness of the material. Equations needed for the calculation of double-K parameters are given in Eqs. 3-8.

$$K_{IC}^{Q} = \frac{3(P_Q + mg \times 10^{-2}) \times 10^{-3} S\sqrt{a_0}}{2bd^2} g(\alpha_0) \tag{3}$$

$$g(\alpha_0) = \frac{1.99 - \alpha_0(1-\alpha_0)(2.15 - 3.93\alpha_0 + 2.7{\alpha_0}^2)}{(1+2\alpha_0)(1-\alpha_0)^{3/2}}, \alpha_0 = \frac{a_0}{h} \tag{4}$$

$$K_{IC}^{S} = \frac{3(P_{\max} + mg \times 10^{-2}) \times 10^{-3} S\sqrt{a_c}}{2bd^2} g(\alpha_c) \tag{5}$$

$$g(\alpha_c) = \frac{1.99 - \alpha_c(1-\alpha_c)(2.15 - 3.93\alpha_c + 2.7{\alpha_c}^2)}{(1+2\alpha_c)(1-\alpha_c)^{3/2}}, \alpha_c = \frac{a_c}{h} \tag{6}$$

where K^S_{IC} is the unstable fracture toughness (MPa.m$^{1/2}$), P_{max} is the initial cracking load (N), S is the span length (m), a_c is the effective critical length (m), b, d and m are the width (m), height (m) and mass (kg) of the specimen.

$$a_c = \frac{2}{\pi}(d + h_0)\arctan\sqrt{\frac{bEV_c}{32.6P_{max}} - 0.1135} - h_0 \quad (7)$$

where h_0 is the thickness (m) of the blade that the extensometer was clipped on; V_c is the critical value of CMOD (μm) that corresponds to maximum load P_{max}, E is the elasticity modulus (GPa).

$$E = \frac{1}{bc_i}\left[3.70 + 32.6\tan^2\left(\frac{\pi}{2}\frac{a_0 + h_0}{d + h_0}\right)\right] \quad (8)$$

where c_i (μm/kN) is the initial compliance calculated from the load–CMOD curve.

3. Results and discussion

3.1. *Flowability*

The flowability diameters of 12 different mortar mixtures were measured and obtained results are expressed in terms of the ratio of the mortar spread diameter to mold base diameter as percentages in Figure 2. Mixtures without fibers were found to have better workability with respect to fibrous mixtures as can be expected. Higher workability was reported for reference mixtures for all SF inclusion levels. Flowability was also found to be decreased with the increasing SF content. The lowest flowability was determined for mixtures with the highest BF and SF content whereas fiber content was found to be the most significant parameter. Although flowability levels differed, MPC mixtures exhibited excellent performance under compaction, according to practitioners. Thus, such various performances may not have resulted in significant variations in the internal structures of the mixtures with lower workability.

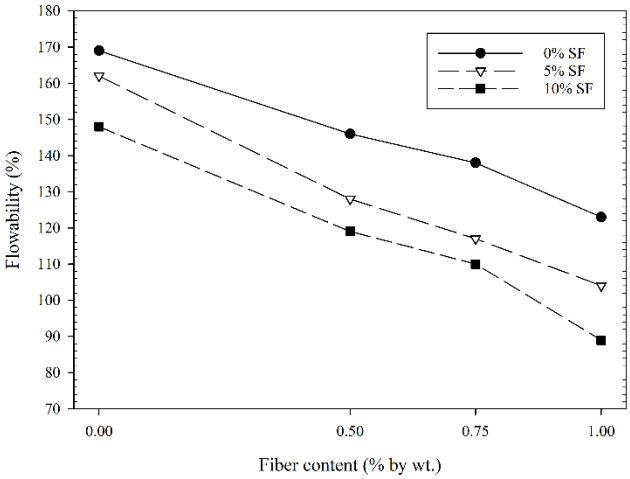

Figure 2. Flowability results of all mixtures.

3.2. *Compressive strength results*

Compressive strength test results are given in Figure 3. All specimens were observed to have good internal bonding mechanism and proper integrity. Moreover, mixtures with SF addition exhibited superior performance creating a denser internal structure thus making a big difference in compressive strength. Specimens with the highest amount of SF were found to have 33% enhancement whereas specimens with 5% SF showed 16% increase. Although control mixture had better flowability results which should be considered as proper compaction and thus fewer voids, the control mixture was unable to supply a dense internal structure. This should be linked with the number of reactions that should have been promoted with the attendance of SF. Therefore, effectiveness due to higher surface area was beyond the microfilling effect of SF, which indicates denser internal microstructure creating higher nucleation sites. The inclusion of SF also enhanced the pore structure resulting in a lower number of large pores (Ahmad & Chen, 2020).

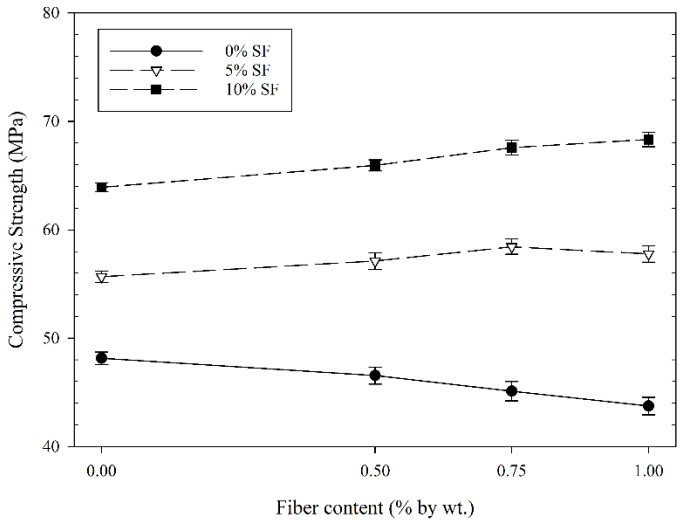

Figure 3. Compressive strength results of all specimens.

Inclusion of BF also changed important characteristics of MPC mixtures. For mixtures without SF addition, the amount of BF lowered the compressive strength which is most probably related to the overall bonding mechanism in these mixtures. These results clearly indicate the effectiveness of SF addition since all mixes with SF addition exhibited apparent enhancement with the increasing fiber amount. Also to promote this behavior, it should be noted that this increase is more effective with a higher percentage of SF addition. Thus, this should be concluded as the net effect of SF addition on the bonding behavior of mixture. When BF addition results are compared, it is seen that effect of BF was observed to be 32 and 56%, respectively for S5BF1 and S10BF1 specimens emphasizing the importance of combined usage of SF and BF together.

3.3. *Compressive strength results*

Splitting strength results are given in Figure 4. As was observed in the compressive strength results, effect of SF addition was more pronounced. By this manner, it should be said that this enhancement level is surely related to the pozzolanic effect of additional micro-sized silica content. SF5 and SF10 specimens have experienced 13 and 21% increases in splitting tensile strength respectively. Effect of BF addition was also observed in splitting tensile strength however, the effect of BF addition was dependent on the amount of SF in the mixture which should be related to the bonding ability of the internal microstructure. Thus, when the effect of BF addition is inspected, it is seen that specimens without SF addition exhibited an increase only with the 0.5% BF content. S0BF0.50 specimens showed the highest splitting resistance between no SF added specimens and supporting the same idea highest level of increase was observed for S5BF0.75 between specimens with 5% SF addition. However, when specimens with 10% SF are investigated, there is a net relationship between the splitting tensile strength and the increasing amount of BF fibers. Thus, also supported with the findings of compressive strength results, specimens with

10% BF addition proved to be a good bonding mechanism and internal microstructure. The highest increase in control specimens was 37.3%, which was observed for S10BF1.00 specimens. To conclude, it should be said that effectiveness of BF was increased with the addition of SF. The addition of SF was found to be helpful in the bonding mechanism that should be related to enhanced bonding strength with the formation of secondary hydration products ($MgSiO_3$) and also aluminium phosphate phases which were detected along the struvite particles improving the bonding mechanism of MPC (Ahmad & Chen, 2020). During splitting accumulation, fibers bridge the split fragments of the specimens resulting into stress transfer from the matrix which is weak in tensile strength to fibers (Kazmi, 2018).

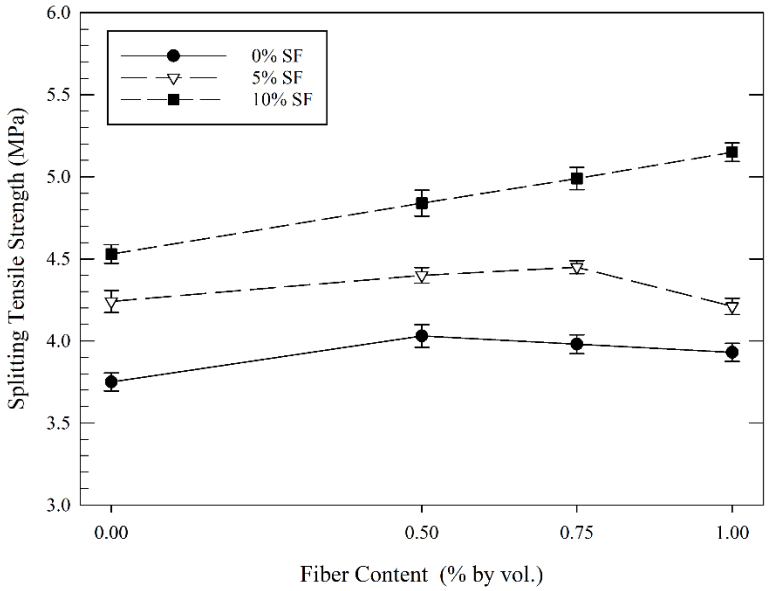

Figure 4. Splitting tensile strength results of all specimens.

3.4. Load-CMOD curve analysis

Load-CMOD curve analysis was facilitated to determine and compare the overall ability to resist fracture of the MPC mixtures. Fracture energy values are given in Figure 5. The inclusion of fibers increased the overall fracture toughness for all mixtures; however, MPC mixtures without any SF addition were not able to exhibit significant development for fracture toughness. Maximum fracture energy increase was noted as 247% concerning control specimens which were seen for S10BF1.00 specimens. These specimens also showed an increase of 157% concerning their non-fibrous versions. S5BF1.00 specimens displayed 189% increase with respect to control specimens and 139% increase with respect to their non-fibrous specimens. When this analysis is made for specimens without SF addition it is seen that relative increase with respect to BF addition was 104% and this increase was similar for all BF addition amounts. Ahmad & Chen (2018) indicated increase in flexural strength with SF inclusion however, no increment in fracture energy was monitored for plain mixtures. An increment in fracture energy was detected for concurrent usage of BF and SF with the ability of higher bonding strength with the inclusion of SF. Zheng et al. (2016) asserted that SF filled the pores in the fibrous mixes, thus creating a denser matrix with improved tensile properties.

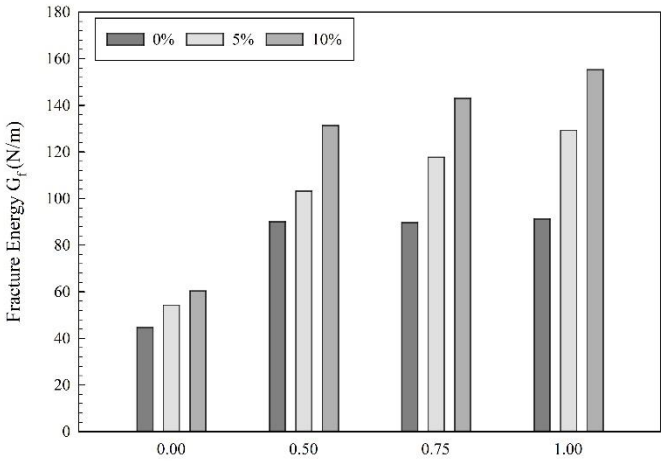

Figure 5. Fracture energy (G_f) values for all specimen series.

Load-CMOD curves are given in Figures 6, 7 and 8. According to load-CMOD analysis, formation and progress of cracks are analyzed in three distinct stages. In Stage 1, linear branch of the loading is observed and it is known that in this stage fibrous composite has not cracked yet. Such that evaluation at this stage is mainly dependent on the matrix rather than reinforcing fibers. However, it should be reminded that presence of fibers in the matrix affect the overall integrity of the matrix and the behavior in Stage I differs with respect to fiber content and thus the elongation in CMOD values. Stage 2 indicates the steady growth of microcracks until the maximum load was reached whereas in Stage 3 after the maximum load interaction between the fibers and the cement matrix is conclusive in the post peak behavior (Sun et al., 2019; Smarzewski, 2020; Pehlivan, 2021). All specimen types have ensured linear phase in the first stage which may be interpreted as the homogenous internal structure for both plain and fibrous mixtures. However, linear phase was ended earlier for fibrous specimens and microcracks were noticed at a lower level of loading with respect to plain specimens. This was clearly observed for specimens with 5% SF addition. However, for specimens with 10% SF addition, although peak loads were higher, matrix failure phase did not exhibit a significant drop in the linearity, which may be an indication of a better fiber-matrix bonding mechanism for specimens with higher SF content. Increased toughness for fibrous composites primarily depends on the sufficient number of fibers to ensure the crack-bridging action (Qin et al., 2018).

Peak strength values and post-peak behavior of all specimen series can be diagnosed from these curves. Between all specimen series highest peak load was detected for specimens with 10% SF addition and they have resisted flexural loading over 2 kN. Lowest peak load was observed for BF10 specimens such that it should be easily asserted that inclusion of SF was highly responsible for resisting higher load levels. It should also be noted that inclusion BF fibers decreased the peak load for series with 0% and 5% SF addition. Thus, inclusion of BF fibers had lower efficiency whereas specimens with %10 SF managed to maintain the peak load levels except 1% BF inclusion. Post-peak behavior was observed to be different than specimens without any fibers. After the peak, these specimens experienced sudden collapse whereas specimens with fibers managed to carry significant loads, decreasing with the increasing crack mouth opening displacement (CMOD).

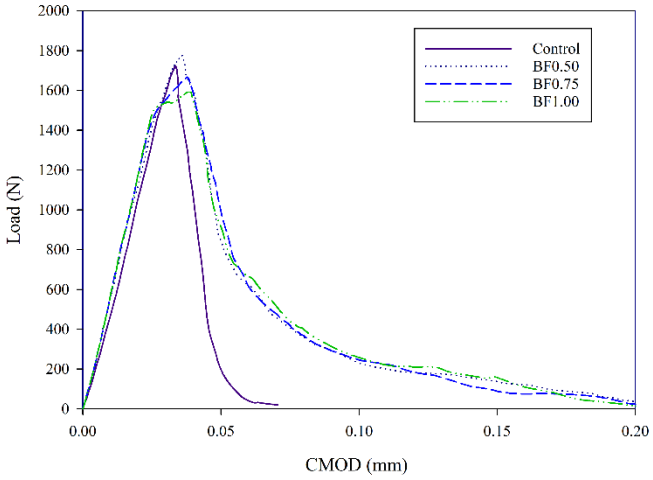

Figure 6. Load CMOD deflection curves for specimens without SF addition.

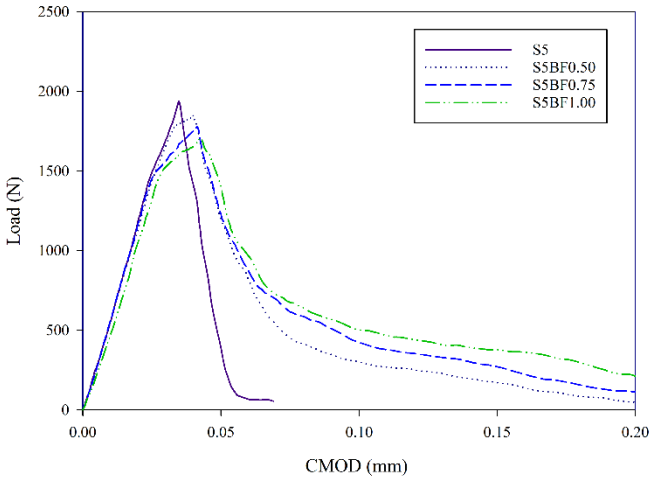

Figure 7. Load CMOD deflection curves for specimens with 5% SF addition.

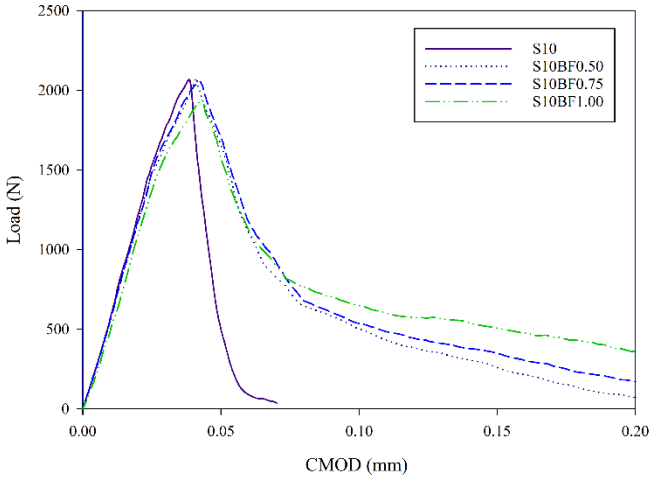

Figure 8. Load CMOD deflection curves for specimens with 10% SF addition.

Modulus of elasticity values are obtained by Eq. 7 using initial compliance values derived from the slope of the load-CMOD curve and given in Figure 9. Lowest MOE values were recorded for control specimens whereas highest value was observed for S10 specimens. Both specimen series were non-fibrous such that it should easily be said that BF fibers were not directly involved in MOE values. MOE range was between 15.75 and 18.15 which makes a total increase of 15%. Regarding this information MOE was not that affected with respect to compressive or splitting tensile strength results.

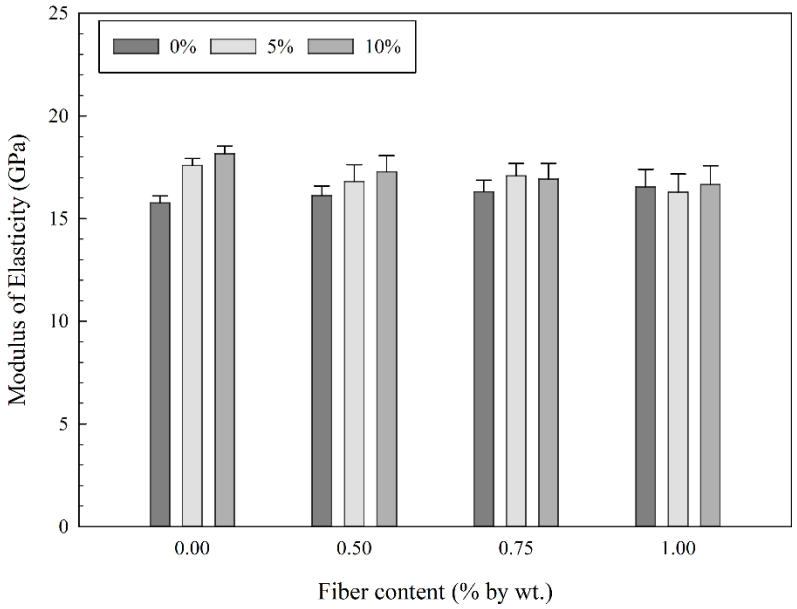

Figure 9. Load CMOD deflection curves for specimens with 10% SF addition.

Interestingly when the results are diagnosed, it is seen that the addition of BF fibers only affected the series with 0 or 0.5 % BF content in positive way however specimens with higher BF content were not enhanced, although SF content was higher. Such that this may be related to the effective bonding with the matrix when BF content was lower and also there may have been several voids due to the existence of multiple fibers in the same vicinity, thus impeding the full-length bonding of the fibers with the matrix.

3.5. Double-K parameters

Double K-parameters are calculated to obtain two different fracture toughness parameters that help to understand and evaluate the response of a material against crack elongation under flexural loading. Crack resistance ability of materials can be monitored easily by using these fracture toughness parameters (Chen et al, 2021). Since toughness measurements were highly dependent on the size of the specimens under examination, size-independent fracture parameters provide healthy info about crack initiation and propagation. Initiation toughness displays the level of toughness at the initial crack width. Beyond this level, cracks grow stably, whereas, over unstable fracture toughness value, the crack starts to grow unstably and eventually, failure of the specimen occurs.

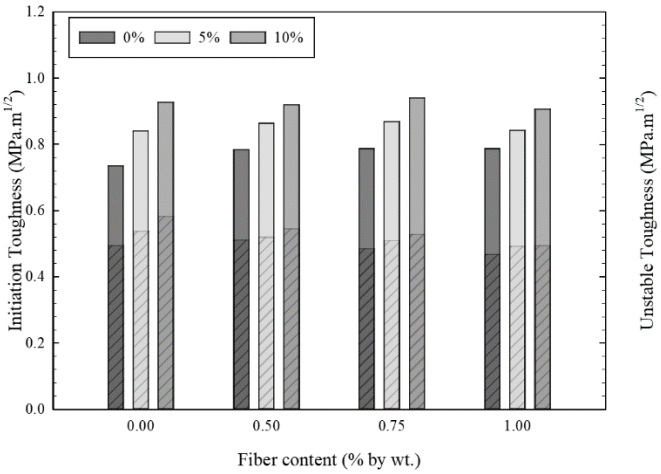

Figure 10. Load CMOD deflection curves for specimens with 10% SF addition.

Double-K parameters were evaluated from the geometrical parameters and the mechanical findings are given in Figure 10. Starting with the overall examination of both toughness values, it is important to see the behavior of fibers in different matrices and it should be said that specimens without any fiber addition exhibited increasing initiation toughness with the increasing SF addition. However, this difference in initiation toughness values was not observed for specimens incorporating BF. Especially for specimens with 10% SF addition, initiation values were decreased by 6.5%, 9.3% and 15% with the increasing BF content respectively. When unstable toughness values are diagnosed, it is seen that highest values were recorded for specimens 10% SF and 0.75% BF which may also be seen as a general finding to discuss the relative ductility of the test specimens. It is observed that with the increasing SF content, unstable toughness values were increased, thus indicating the net effect on the matrix structure and integrity.

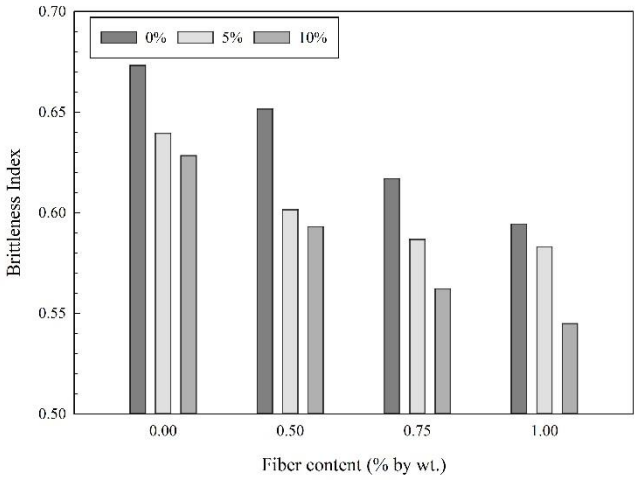

Figure 11. Brittleness index values for all specimen series.

The brittleness index is used to measure the relativeness of initiation toughness to unstable toughness as was proposed by Kumar & Barai (2009). Brittle index value is used to evaluate the ductility of the specimen. As may be interpreted by the name, if brittle index is high then brittleness of the specimen is higher; if it is low then the ductility of the specimen is higher. So, this index helps to conclude the experimental findings of the notched flexural testing independent of the size of the specimens used in testing. When the brittleness index values given in Figure 11 are examined, it is seen that lowest ductility was seen for control series. With the increase of SF addition in the matrices, all specimens showed significant development in ductility. In addition, this was also amplified with the addition of BF content especially for specimens with 10% SF and 1% BF. Such that lowest brittleness index was observed for S10BF1.0 specimens. Existence of high content of BF should only be compensated with a dense matrix that incorporate significant amount of SF. Specimens without SF addition were not found to be ductile enough although they incorporate BF which may be related to the weaker bonding between the matrix and the fibers.

Critical crack length (a_c) values are used in calculating the size-independent fracture parameter results such that these findings are also beneficial to diagnose since they reflect the actual size parameter that does not depend on the size of the tested specimens. Critical crack length is also an important parameter defining the crack length triggering the unstable crack growth. Critical crack length findings are given in Figure 12. Highest crack length was observed for specimens with highest BF content. Fibers increased the resistance to sliding of micro-cracks, thus reducing the wing-crack growth (Kazmi et al, 2018). Critical crack length was lowest for control series specimens which should be interpreted as the lowest ability to attain crack before failure. Matrices with 0 and 5 % SF addition attributed good contribution to critical crack length, whereas 10 % SF addition did not exhibit a good increase whether the fiber content is high or not.

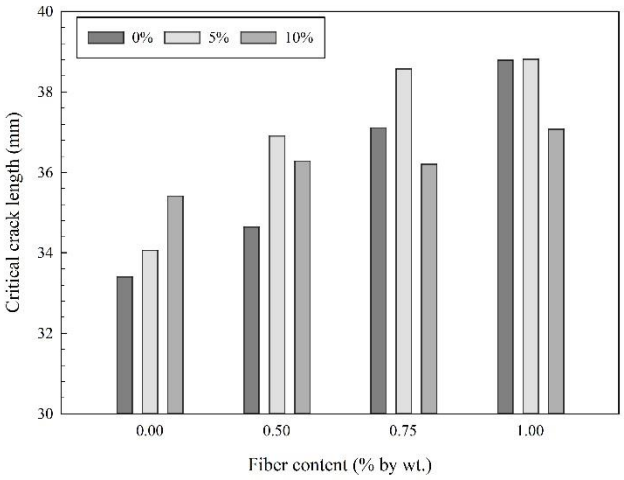

Figure 12. Critical crack length (a_c) for all specimen series.

4. Conclusions

In this study, specimens with increasing content of BF in varying lengths were examined to illustrate the effect of the fibers on mechanical properties and particularly size-independent double-K parameters. For fracture toughness, testing notched beam specimens were used and cracked under flexural loading and crack mouth opening displacement data were recorded simultaneously. Several findings were found for the behavior of concrete incorporating BF and summarized as follows:

1. Compressive strength of specimens incorporating BF were not found to be enhanced however in some specimen series, a maximum 4% increase was detected. Standard deviation results were close to plain specimens that define the proper placement despite the presence of fibers.
2. Tensile properties showed high development for both splitting tensile and flexural testing. However, effect of the two parameters was different for flexure and splitting. Although 6 mm fiber specimens seemed more problematic for overall mechanical properties, splitting tensile results were relatively convincing for these short fibers.
3. Splitting tensile and flexural test results were enhanced by 28% and 22%, respectively. The modulus of elasticity results obtained from the notched three-point bending test also agreed with the mechanical testing results.
4. Highest fracture energy was measured for specimens with 1% content of 24 mm fibers displaying an increase of 37% with respect to plain specimens. Energy dissipation of shorter fibers was less compared to medium and long fibers.
5. Double-K fracture parameters were found to be coherent with other studies in the literature, and these parameters demonstrated good results regarding fracture capability. Higher unstable toughness values proved a good measure of strain-attaining capacity regardless of specimen size.
6. Brittleness index also showed that fiber content was the dominant parameter regarding material toughness. Additionally, fiber length was also found to be influential in determining fracture process and energy dissipation.

For future work, by using different specimen size variations, toughness findings should be checked if the size effect is indeed eliminated or not for these types of cementitious materials.

Funding: There was no funding in this project.

Conflicts of interest: There were no conflicts of interest.

References

Ahmad, M. R., & Chen, B. (2018). Effect of silica fume and basalt fiber on the mechanical properties and microstructure of magnesium phosphate cement (MPC) mortar. Construction and Building Materials, 190, 466–478.

Ahmad, M. R., & Chen, B. (2020). Microstructural characterization of basalt fiber reinforced magnesium phosphate cement supplemented by silica fume. *Construction and Building Materials*, *237*, 117795.

Aminul Haque, M., Chen, B., Riaz Ahmad, M., & farasat ali shah, S. (2020). Mechanical strength and flexural parameters analysis of micro-steel, polyvinyl and basalt fibre reinforced magnesium phosphate cement mortars. *Construction and Building Materials*, *235*, 117447.

Araya-Letelier, G., Maturana, P., Carrasco, M., Antico, F. C., & Gómez, M. S. (2019). Mechanical-damage behavior of mortars reinforced with recycled polypropylene fibers. *Sustainability*, 11(8), 2200.

ASTM 1437. (2005). Test method for slump of hydraulic cement concrete. *American Society for Testing and Materials*, 12–15.

ASTM C1018. (1997). Standard Test Method for Flexural Toughness and First-Crack Strength of Fiber-Reinforced Concrete (Using Beam with Third-Point Loading). ASTM International, West Conshohocken, PA, United States. 04, 1–8.

ASTM C496. (2008). Standard Test Method for C. Standard Test Method for Splitting Tensile Strength of Cylindrical Concrete Specimens1, 334-334–3.

ASTM C39. (2003). Standard Test Method for Compressive Strength of Cylindrical Concrete Specimens 1. *ASTM Standard Book*, *04*(March), 1–5.

Chen, W., Peng, L., & Yang, H. (2021). Fracture behaviors of concrete incorporating different levels of recycled coarse aggregate after exposure to elevated temperatures. Journal of Building Engineering, 35(September 2020), 102040.

Fang, Y., Chen, B., & Oderji, S. Y. (2018). Experimental research on magnesium phosphate cement mortar reinforced by glass fiber. Construction and Building Materials, 188, 729–736.

FMC-50R. (1985). UV-spectroscopic study of complex formation by certain cycloolefins with tetracyanoethylene and molecular iodine. *Materials and Structures*, *18*(6), 287–299.

Hall, D. A., Stevens, R., & El-Jazairi, B. (2001). The effect of retarders on the microstructure and mechanical properties of magnesia-phosphate cement mortar. *Cement and Concrete Research*, *31*(3), 455–465.

Han, W., Chen, H., Li, X., & Zhang, T. (2020). Thermodynamic modeling of magnesium ammonium phosphate cement and stability of its hydration products. *Cement and Concrete Research*, *138*(June), 106223.

Hillerborg, A., Modéer, M., & Petersson, P. E. (1976). Analysis of crack formation and crack growth in concrete by means of fracture mechanics and finite elements. *Cement and Concrete Research*, *6*(6), 773–781.

Jenifer, J. V., & Brindha, D. (2021). Development of hybrid steel-basalt fiber reinforced concrete - in aspects of flexure, fracture and microstructure. *Revista de La Construccion*, *20*(1), 62–90.

Kazmi, S. M. S., Munir, M. J., Wu, Y. F., & Patnaikuni, I. (2018). Effect of macro-synthetic fibers on the fracture energy and mechanical behavior of recycled aggregate concrete. Construction and Building Materials, 189, 857–868.

Kumar, S., & Barai, S. V. (2009). Determining double-K fracture parameters of concrete for compact tension and wedge splitting tests using weight function. Engineering Fracture Mechanics, 76(7), 935–948.

Li, Y., & Chen, B. (2013). Factors that affect the properties of magnesium phosphate cement. Construction and Building Materials, 47, 977–983.

Mo, L., Lv, L., Deng, M., & Qian, J. (2018). Influence of fly ash and metakaolin on the microstructure and compressive strength of magnesium potassium phosphate cement paste. Cement and Concrete Research, 111(30), 116–129.

Qin, J., Qian, J., Li, Z., You, C., Dai, X., Yue, Y., & Fan, Y. (2018). Mechanical properties of basalt fiber reinforced magnesium phosphate cement composites. *Construction and Building Materials*, *188*, 946–955.

Ribeiro, D. V., Paula, G. R., & Morelli, M. R. (2019). Effect of boric acid content on the properties of magnesium phosphate cement. *Construction and Building Materials*, *214*, 557–564.

Sasaki, K., & Moriyama, S. (2014). Effect of calcination temperature for magnesite on interaction of MgO-rich phases with boric acid. *Ceramics International*, *40*(1 PART B), 1651–1660.

Sateshkumar, S. K., Awoyera, P. O., Kandasamy, T., Nagaraj, S., Murugesan, P., & Ponnusamy, B. (2018). Impact resistance of high strength chopped basalt fibre-reinforced concrete. *Revista de La Construccion*, *17*(2), 240–249.

Smarzewski, P. (2020). Flexural toughness evaluation of basalt fibre reinforced HPC beams with and without initial notch. *Composite Structures*, *235*(December 2019), 111769.

Sun, X., Gao, Z., Cao, P., Zhou, C., Ling, Y., Wang, X., Zhao, Y., & Diao, M. (2019). Fracture performance and numerical simulation of basalt fiber concrete using three-point bending test on notched beam. *Construction and Building Materials*, *225*, 788–800.

Xu, S., & Reinhardt, H. W. (2000). A simplified method for determining double-K fracture parameters for three-point bending tests. *International Journal of Fracture*, *104*(2), 181–209.

Xu, S., & Reinhardt, H. W. (1999). Determination of double-K criterion for crack propagation in quasi-brittle fracture, Part I: Experimental investigation of crack propagation. *International Journal of Fracture*, *98*(2), 111–149.

Yang, N., Shi, C., Yang, J., & Chang, Y. (2014). Research Progresses in Magnesium Phosphate Cement–Based Materials. *Journal of Materials in Civil Engineering*, *26*(10), 04014071.

Zhang, T., Chen, H., Li, X., & Zhu, Z. (2017). Hydration behavior of magnesium potassium phosphate cement and stability analysis of its hydration products through thermodynamic modeling. *Cement and Concrete Research*, *98*(June 2016), 101–110.

Zheng, D. D., Ji, T., Wang, C. Q., Sun, C. J., Lin, X. J., & Hossain, K. M. A. (2016). Effect of the combination of fly ash and silica fume on water resistance of Magnesium-Potassium Phosphate Cement. *Construction and Building Materials*, *106*, 415–421.